

FibrilGen: A Python Package for Atomistic Modeling of Peptide β -Sheet Nanostructures

Chao-Yu Yang, Aline F. Miller, Alberto Saiani, and Richard A. Bryce*



Cite This: <https://doi.org/10.1021/acs.jcim.5c02108>



Read Online

ACCESS |

Metrics & More

Article Recommendations

Supporting Information

ABSTRACT: For *de novo* peptide-based nanomaterials that rely on the rational design of the peptide primary sequence, a systematic approach to computationally model the diverse and complex potential nanostructures formed by self-assembling peptides would be of considerable value. Here, we present FibrilGen, a bespoke Python package capable of building a broad range of cross- β morphologies at the atomic level. FibrilGen takes a set of input geometrical parameters to initialize peptide packing and fibril morphology, followed by a refinement step to produce a compact assembly. Using FibrilGen, one can, for example, generate a variety of assembled cross- β structures as input for molecular simulations; the package also includes features for geometric analysis of fibril nanostructures and their associated trajectories. We demonstrate the utility of the tool by generating cross- β nanostructures of varying morphologies that compare well with self-assembled arrangements determined from cryogenic electron microscopy and solid state nuclear magnetic resonance spectroscopy. These structures also exhibit conformational stability over microsecond molecular dynamics simulations in aqueous solution. We further assess the capability of the modeling/simulation pipeline to filter out nonexperimental β -sheet fibril structures. Thus, the FibrilGen package provides a route to construction of atomistic supramolecular peptide structures of a variety of possible morphologies, for visualization, simulation, and assessment of interactions and stability.



top-down modeling of helical β -sheet nanostructures

1. INTRODUCTION

The use of noncovalent supramolecular assembly has become a prominent strategy, offering practical routes for the construction of increasingly functional nanomaterials across a variety of applications.¹ For the molecular building blocks used for this purpose, one that has attracted considerable attention in the last 20 years is the *de novo* designed self-assembling peptide (SAP). Although at first SAPs were mainly studied for the role they play in disorders such as Alzheimer's or Parkinson's disease, in the past two decades, scientists have investigated the possibility of exploiting the self-assembly properties of these short natural molecules to design novel materials.² There are a variety of SAP have been developed over time, including amphiphilic peptides, short peptide derivatives, and α -helix- and β -sheet-forming peptides.^{3–9} The latter has become particularly favored in the biomedical field, as it allows the design of biocompatible and shear-thinning fibrillar hydrogel scaffolds that show potential for use in a range of applications, from cell and organoid 3D *in vitro* culture to drug delivery *in vivo*.^{10–14}

The fundamental features of a cross- β structure formed by SAPs are well-known: the peptides assemble into unidirectional cross- β ladders, parallel or antiparallel depending on the relative orientation of the peptides, with an intrasheet backbone interpeptide spacing of 4.8–4.9 Å, and are stabilized by intermolecular hydrogen bonding.^{15–17} Despite the

simplicity of the assembly at the peptide molecular level, these SAPs can form extended supramolecular assemblies with a broad variety of morphologies, from thin and thick fibers to tubes, ribbons and tapes.^{4,18} Despite the significant amount of work done to elucidate the morphology of these structures using state-of-the-art techniques such as cryogenic electron microscopy (cryo-EM),¹⁵ X-ray diffraction (XRD)¹⁶ and solid state nuclear magnetic resonance (ssNMR),¹⁷ the correlations between peptide sequence and final supramolecular structure morphology are still poorly understood. Not only does the final self-assembled structure depend on the peptide sequence itself, environmental factors such as media pH and ionic strength, solvent polarity and temperature also play key roles in dictating the morphology of the final supramolecular assembly.^{5,6,19}

Supramolecular assemblies can be reconstructed from experiment by several software packages: RELION²⁰ for example allows single particle analysis of cryo-EM images to reconstruct electron density. ROSETTA²¹ provides rigid-body

Received: September 1, 2025

Revised: September 24, 2025

Accepted: September 26, 2025

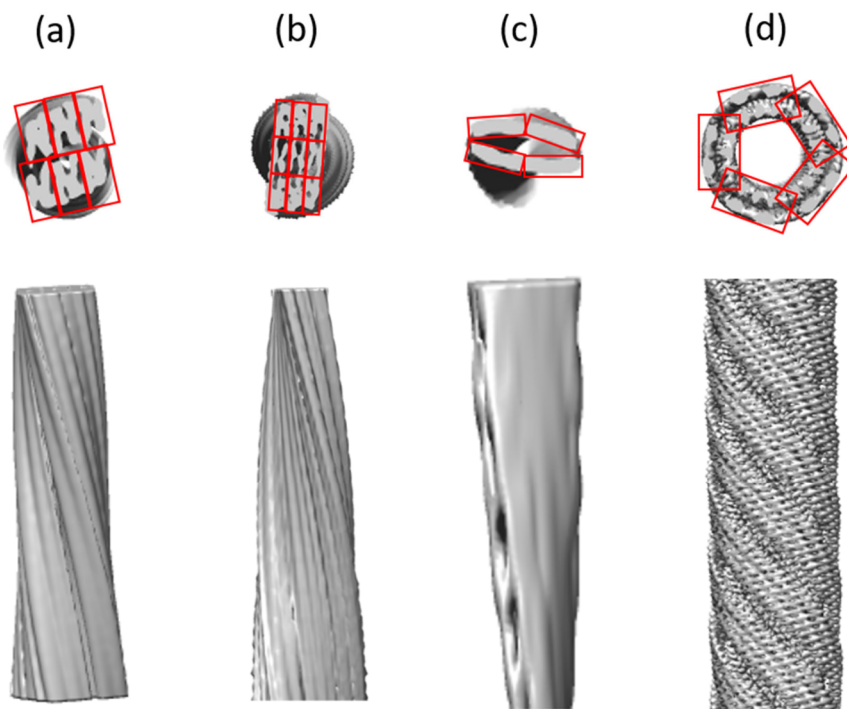


Figure 1. Common periodic building blocks of β -sheet bilayer (red boxes) for cross- β fibrils: (a) 12-mer peptide (IGSNVVTWYQQL, denoted AL1) for six stacking parallel β -sheet bilayers, forming a left-handed rod morphology.²⁸ (b) AL1 peptide for nine stacking parallel β -sheet bilayers, forming a left-handed rod.²⁸ (c) 11-mer peptide (YTIAALLSPYS) which forms parallel β -sheets, assembled into a left-handed tube.²⁹ (d) 8-mer peptide (FKFEFKFE with N-terminal acetylation and C-terminal amidation, denoted HP8) which forms parallel β -sheets or antiparallel β -sheets, assembled into a left-handed tube.¹⁸ Electron densities visualized with Chimera 1.17.3.³⁰

transformation of molecules into symmetrical assemblies to model NMR or cryo-EM data. PHENIX²² supports inference of atomistic models from X-ray and neutron diffraction and cryo-EM data. The molecular dynamics flexible fitting (MDFF) method²³ samples low energy structures from molecular dynamics simulations confined by cryo-EM density maps; however, fitting to low resolution data can be problematic. For molecular modeling without fitting to experimental constraints, a variety of software programs are available to pack molecules into specific assembly patterns. For example, PACKMOL²⁴ can assemble molecules into spheres, ellipses, cylinders, planes, or boxes. Polyphy²⁵ can perform a self-excluding random walk of coarse-grained beads in order to generate polymer conformations. Nanomaterial Modeler²⁶ contains a unit cell library to enable assembly of bulk metal, mineral and carbonaceous materials. While these modeling packages are valuable for building molecular assemblies, there is a need for a bespoke tool to construct unidirectional supramolecular structures in cross- β arrangements that span a wide range of complex, experimentally observed morphologies.

In this regard, we have developed the FibrilGen Python library, designed to build supramolecular rod and ribbon structures formed by β -sheet-forming SAPs in various arrangements. The library conveniently can be called from within the visualization package, PyMol,²⁷ for rapid conceptualization of proposed structures. In FibrilGen, the elementary building block of four peptides is taken to model various steric zippers in cross- β structures.^{16,18} The motif of four peptides, *i.e.* two β -strands in a β -sheet and then two of these β -sheets together to form a bilayer, contains the essential backbone hydrogen bonding and side chain packing to stabilize the overall bilayer structure. Moreover, FibrilGen introduces

geometrical operations of twisting and stacking to guide supramolecular assembly of the bilayer structure. To conveniently generate a range of cross- β nanostructures from this motif, FibrilGen allows several geometrical parameters to be controlled, followed by an automatic refinement of input parameters to remove steric clashes and produce a compact assembly. The resulting model can then provide input into molecular simulation programs for further refinement of the cross- β nanostructure in the condensed phase.

To exemplify the ability of FibrilGen to construct diverse cross- β nanostructure assemblies at the atomic level, we reconstruct and compare these with three experimentally characterized cross- β systems of differing morphology. We show that the atomistic models generated by FibrilGen agree well with the observable backbone packing derived from ssNMR and cryo-EM data. We further simulate these FibrilGen atomistic models in explicit solvent using microsecond molecular dynamics (MD) simulations: we find that the peptide orientation and overall morphology of the cross- β nanostructures remain in stable conformations over replicate microsecond trajectories at 300 K. The capability of our modeling pipeline to systematically assess hypothetical structures is also investigated. In this regard, a range of nonexperimental peptide assemblies is explored using the workflow. As a computationally expedient tool integrated with PyMol, FibrilGen has the potential to facilitate workflows for the design of cross- β sheet forming SAPs and visualization of their putative atomistic nanostructures of varying morphology.

2. METHODS

2.1. FibrilGen Architecture.

Cross- β fibrils reconstructed from cryo-EM images show that their constituent peptides

assemble into ladder-like β -sheets, and that the faces of two of these β -sheets stack together into a two-sheet bilayer.¹⁶ Examples of cross- β fibrils include 12-mer peptide IGSNVVTWYQQL, denoted AL1 (Figure 1a,b),²⁸ 11-mer peptide YTIAALLSPYS (Figure 1c),²⁹ and 8-mer peptide Ac-FKEFKF-NH₂, which we denote here as HP8 (Figure 1d).¹⁸ As can be seen from these structures, the two-sheet bilayers can form higher order associations of, e.g., four, five, six, and nine of these bilayers (red boxes, Figure 1); and can form rod-like (Figure 1a,b) and tube-like (Figure 1c,d) morphologies. The atomistic modeling of these potential combinations of bilayers into higher order (Figure 1c,d) and often multilayered (Figure 1a,b) geometries can be a challenging undertaking.

Here, we introduce the FibrilGen python library to enable the construction of diverse cross- β nanostructures with seven geometrical parameters (Table 1). The tool supports the

infeasible conformations (Section 2.4). To provide a rapid *in silico* route to conceptualization of potential cross- β nanostructure models, we implement FibrilGen as a Python library which the user can call from the PyMOL command line²⁷ (Supporting Information), enabling convenient visualization of the generated atomistic assemblies.

2.2. FibrilGen Assembly Unit. In FibrilGen, a range of twisted, multilayered fibril morphologies are assembled by a given 2×2 peptide unit cell. For simple combinatorial assembly of the 2×2 unit, we provide a script, *pep2unit*, to assemble four copies of an input peptide (Figure 3a) by the following options: the intersheet alignment of two β -sheets in the xz -plane as face-to-back or face-to-face (Figure 3b); the intrasheet alignment between neighboring β -strands as in-register or out-of-register with a shift along the x -axis (Figure 3c); the two-sheet structure as composed of parallel or antiparallel β -sheet (Figure 3d). In construction of the 2×2 units of this study, for each amino acid, the dihedral angle, χ_1 , around the side-chain $C_\alpha-C_\beta$ bond, is assigned to maintain reasonable inter-residue distances and avoid steric clashes between atoms. Given that a β -strand alternates side chains between two sides of the β -sheet, the neighboring C_β atoms on the same side are separated by 7.3 Å. A simple choice is to initialize χ_1 as 80° (closer to N-terminus) or 160° (closer to C-terminus) to maximize the separation between side chains. If steric clashes occur subsequent to this, then the χ_1 of those specific side chains can be manually adjusted. Further side chain optimization at this point could be possible using a conformational search package. Here, we choose energy minimization to refine the side chain packing.

Therefore, as part of the workflow and to assess the feasibility of the assembly produced by the 2×2 unit, a β -sheet bilayer structure of five repeats of the 2×2 unit is built, and this two-sheet structure is energy minimized in explicit solvent using the AMBER molecular simulation package.³¹ The peptides are modeled by the ff14SB force field,³² and water with the TIP3P model,³³ along with Na⁺ or Cl⁻ to neutralize the system. Given a relaxed, solvated β -sheet bilayer structure, a centrally located 2×2 unit is selected to form the elementary building block for assembling further cross- β nanostructures.

Table 1. Description of Seven FibrilGen Geometrical Parameters and Use (Y/N) to Model Rod and Ribbon Structures

parameter	description	rod model	ribbon model
N	Number of units to extend along fibril long axis	Y	Y
K	Binary matrix of stacking pattern on fibril cross-section	Y	N
M	Number of units to fit in a rotational pattern in fibril cross-section plane	N	Y
θ_s	Angle of rotation, to repeat units in fibril cross-section plane (deg)	N	Y
θ_z	Tilt angle, to angle units from fibril axis (deg)	Y	Y
r_y/r_s	Pore radius, to displace units from fibril axis (Å)	Y	Y
θ_y	Twist angle, to rotate successive units along fibril axis (deg). The sign of θ_y is 1 for a left-handed chirality, and -1 for a right-handed chirality.	Y	Y

composition of a β -sheet bilayer of four β -strands in parallel/antiparallel alignments (Figure 2a); and the assembly of the β -sheet bilayer into a range of fibril nanostructures via stacking (Figure 2b) and twisting (Figure 2c) operations, with iterative resolution of interpeptide spacing to exclude geometrically

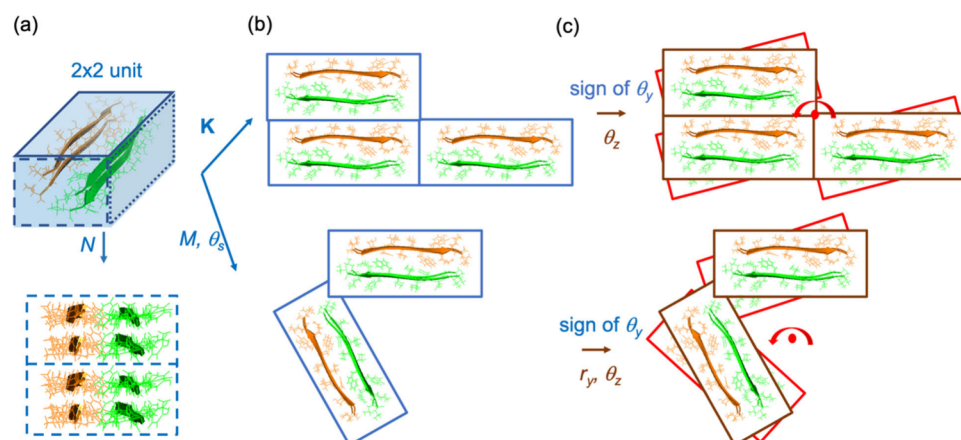


Figure 2. Modeling scheme in FibrilGen. A set of input parameters can be controlled by users: (a) A periodic basis of 2×2 unit and a repeat of N along the β -sheet axis. (b) A stacking of the 2×2 unit on the fibril cross-section, with a matrix K to contact the edges of the units or a repeat of M with angle θ_s to contact the corner of the units. (c) The sign for a twist angle θ_y around the β -sheet axis and a tilt angle θ_z from the β -sheet axis (and a radius r_y from the β -sheet axis). Users can assign a stacking pattern (by N , K , M , θ_s) and an initial helical twist (by the sign of θ_y , r_y , θ_z) for FibrilGen to refine the helical twist and assemble into a compact and nonintersecting fibril structure.

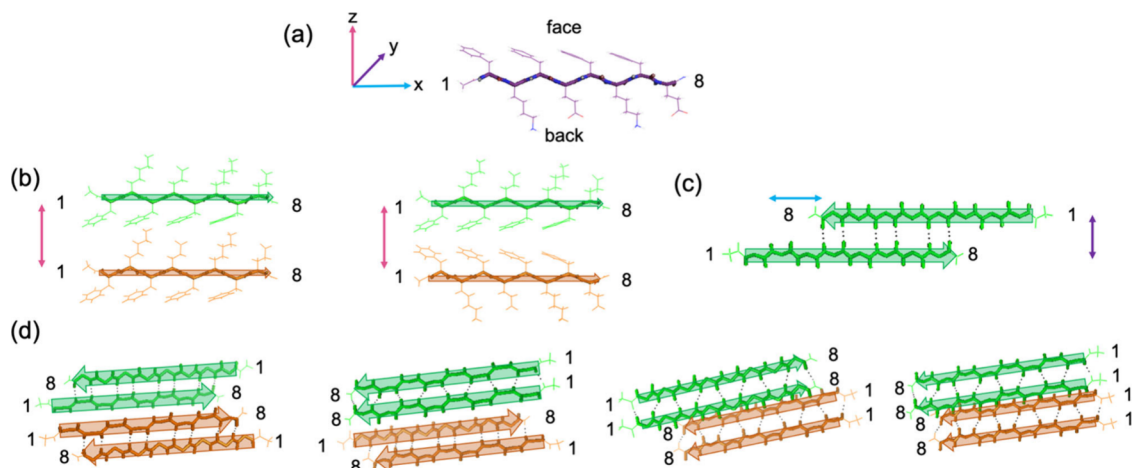


Figure 3. Assembly of 2×2 peptide units. Given an input peptide such as (a) Ac-FKFEFKFE-NH₂, the *pep2unit* script can be used to align the peptide into two β -sheets (green, orange), with the options below: (b) An intersheet alignment of the two β -sheets (the intersheet spacing is labeled in pink) on the *xz*-plane to be (left) face-to-back or (right) face-to-face. (c) An intrasheet alignment of neighboring β -strands with a register (blue) along the *x*-axis and a shift of 4.8 Å (purple) along the *y*-axis. (d) Parallel/antiparallel alignment of antiparallel (labeled as β_a) and parallel (labeled as β_p) β -sheets: two antiparallel aligned β_a (labeled as $\beta_a\beta_a$), one β_p and one β_a aligned antiparallel (labeled as $\beta_p\alpha\beta_a$), two antiparallel aligned β_p (labeled as $\beta_p\beta_p$), and two parallel aligned β_p (labeled as $\beta_pp\beta_p$). Here, in-register β -sheets in face-to-face alignment are taken as an example.

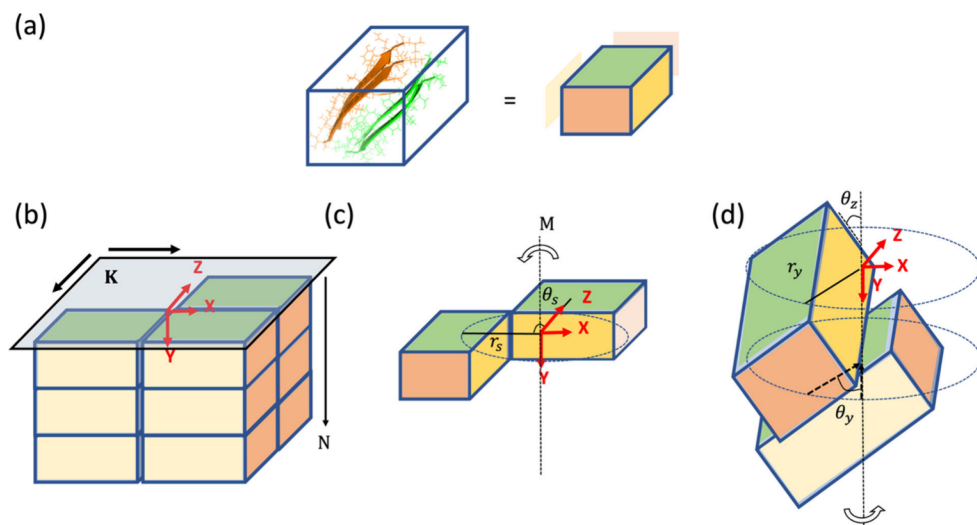


Figure 4. Assembly operations in FibrilGen. (a) 4-Peptide elementary assembly unit (represented as a box) is assembled into nanofibrils by affine transformation. (b) An operation called linear stacking is introduced to contact the faces of boxes, using *K* to arrange elementary units on the fibril cross-section or *N* to extend the fibril length. (c) An operation called rotational stacking is introduced to contact the edges of boxes, using a radius of *r_s*, a twist angle of θ_s to stack the units for *M* times around the fibril axis. (d) An operation called twisting is introduced to adjust face contacts of boxes along the fibril axis, using a radius of *r_y*, a twist angle of θ_y and a tilt angle of θ_z to rotate around the fibril axis.

2.3. FibrilGen Assembly Parameters. The FibrilGen library supports the assembly of cross- β nanostructures in rod morphologies, where flat sheets are a special case; or ribbon morphologies, where tubes are a special case. To model this, FibrilGen uses seven geometrical parameters *N*, *K*, θ_s , *M*, *r_y*, θ_y and θ_z (Figure 4, Table 1). These define the packing of the assembly unit (Figure 3a) on the fibril long axis, defined as the *y*-axis, and the fibril cross-section, defined as the *xz*-plane (Figure 3b).

The parameters *N*, *K*, θ_s and *M* define the stacking pattern of the assembly unit. A positive integer *N* defines the number of elementary units to be assembled along the *y*-axis. For a binary matrix *K* to represent a linear stacking in the *xz*-plane (Figure 4b), the dimensions of *K* are assigned by the maximum repeat of units on the *x*-axis and *z*-axis, and each entry of *K* controls

whether a stacked unit is present (value of 1) or not (value of 0). So, in Figure 4b for example, the matrix $K = \begin{pmatrix} 0 & 1 \\ 1 & 1 \end{pmatrix}$ which corresponds to a maximal repeat on the *x*-axis of 2; a maximal repeat on the *z*-axis of 2; and for the upper left corner, a stacked unit is absent. For rotational stacking in the *xz*-plane (Figure 4c), the assembly unit is displaced from the *y*-axis by radius of rotation, *r_s*. *M* is the number of units to populate a rotational pattern in the *xz*-plane, such that a rotational angle *i*· θ_s is applied to unit *i* around the fibril long axis for *i* = 0, 1, 2, . . . *M*-1.

Parameters θ_z , *r_y* and θ_y determine the helical twist of the nanostructure (Figure 4d). Each assembly unit *i* is successively twisted by (1) rotation around the *z*-axis by angle θ_z , (2) then translation along the *z*-axis by distance *r_y*, and (3) rotation

around the y -axis by $i \cdot \theta_y$. This is accompanied by an internal additional rotation of $\theta_y/2$ applied within the 2×2 unit, between the lower and upper peptides within the β -sheets to bridge the twist and maintain the intrasheet hydrogen bonding with adjacent units. Finally, (4) translation is performed along the y -axis by $i \cdot 2b \cos \theta_z$, where b is a constant of 4.8 \AA to maintain a suitable intrasheet hydrogen bonding distance between neighboring units.^{15–17}

Five of these seven parameters are required to assemble rod-like cross- β fibril structures (Table 1, Figure 5a,b). A rod

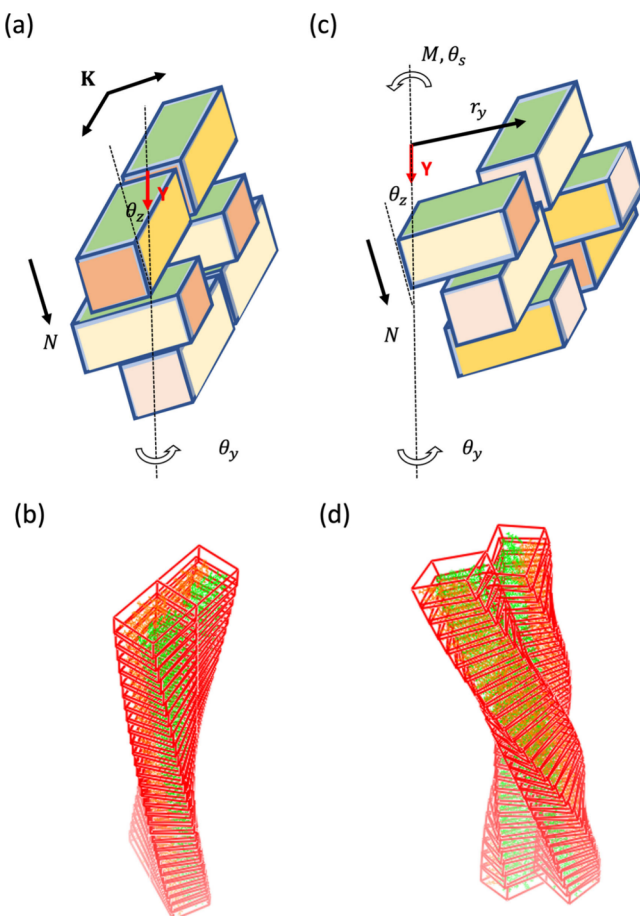


Figure 5. Essential morphological models in FibrilGen: (a) Basis of rod model built via linear stacking and twisting. (b) Example of extended box stacking to produce a rod model. (c) Basis of ribbon model built via rotational stacking and twisting. (d) Example of extended box stacking to produce a ribbon model.

nanostructure is generated by a combination of a linear stacking of K in the xz -plane, a linear stacking of N on the y -axis, and a twisting of r_y , θ_z and θ_y along the y -axis (Figure 5b). The fibril long axis for rotating the assembly units passes through the center of K ; therefore, here r_y is fixed. Without a helical twist (such that θ_z and θ_y are zero), the rod would be reduced morphologically to a flat sheet.

Six of the seven parameters are needed to create a ribbon-like model using FibrilGen (Table 1, Figure 5c,d). A ribbon nanostructure is created using a combination of rotational stacking via M and θ_s , a linear stacking of N on the y -axis, and a twisting of r_y , θ_z and θ_y along the y -axis (Figure 5c). Here, r_s is equal to r_y so that rotational stacking (Figure 4c) is synchronized with helical twisting (Figure 4d) in the same

rotation circle. A special case of the ribbon is a tube, where θ_s : $M = 360^\circ$.

2.4. FibrilGen Structural Refinement. The method of packing refinement in the process of assembling 2×2 units is next considered. Given an arbitrary initialization of geometrical parameters assigned from users, FibrilGen provides incremental refinements of helical twist to achieve a compact assembly complex without a steric clash between atoms. In this way, the method filters out infeasible twists for the given β -sheet stacking. To define a helical twist, parameters of twist angle θ_y , tilt angle θ_z and radius r_y are related by eq 1:

$$(b \cdot \cos \theta_z)^2 + (r_y \sqrt{2 - 2 \cos \theta_y})^2 = b^2 \quad (1)$$

where constant b is the spacing of consecutive peptides within a β -sheet. In eq 1, the first term is the squared distance of the projection of spacing b along the fibril long axis, while the second term is derived from projection of spacing b onto the fibril cross-section. For adjacent peptides to rotate around the circle of radius r_y , the distance is $2 \cdot r_y \cdot \sin(\theta_y/2)$. With several substitutions of trigonometric functions, this distance is equivalent to $r_y \sqrt{2 - 2 \cos \theta_y}$.

The refinement of helical twists depends on the set of conditions below. The first condition, to preserve a minimum tilt, is that the helical tilt angle $\theta_z > \theta_{z,min}$; this constant has a default value of 1.14° and can be reassigned by users. The second condition, to avoid steric clashes, is that the helical twist angle θ_y is > 0 and $< \theta_{y,max}$. Here, the constant $\theta_{y,max}$ is set by increasing the twist angle until any interatomic distance is smaller than a predefined constant. The final condition, to ensure a proper rotational stacking of neighboring β -sheets, is that the nearest distance between atoms from neighboring β -sheets is $> 2 \text{ \AA}$ and $< 5 \text{ \AA}$.

Starting from the user assigned geometry, FibrilGen iteratively refines the helical twist until the geometrical conditions are satisfied. Here, we require rods to satisfy the first two conditions; if not then the tilt angle θ_z is gradually decreased in increments of 0.02 rad . For ribbons, we require all conditions to be satisfied; if not, then the tilt angle θ_z is gradually adjusted by 0.02 rad , with addition to the pore radius r_y of a small amount of noise $\leq 1 \text{ \AA}$. The iterative refinement of θ_z (and r_y) terminates once the conditions are satisfied or the maximum number of iterations is reached (by default set as 40).

The usage of input geometrical parameters to generate a diverse range of fibril nanostructures is implemented into six FibrilGen functions (details in Supporting Information). Guidelines on using FibrilGen to explore fibril assembly are also provided there. Examples of creating different morphologies are provided in Figures S10 and S11.

2.5. Molecular Dynamics Simulations and Structural Analysis. Molecular dynamics simulations were used to assess the stability of cross- β nanostructures in explicit aqueous solvent at 300 K . Three cross- β systems were constructed based on the experimental information: a 10-sheet hydrogel tube formed by peptide HP8;¹⁸ a 12-sheet rod of peptide AL1;²⁸ and third, a 2-sheet rod of amyloid- β peptide, $A\beta_{42}$,³⁴ a structure implicated in Alzheimer's disease which has been targeted by β -sheet breaker compounds.³⁵ Two other cross- β systems that were not observed experimentally were also constructed: a 12-sheet rod comprised by peptide HP8 (two different charge states are considered); and a 2-sheet tube of peptide AL1. Further details of their assembly are provided

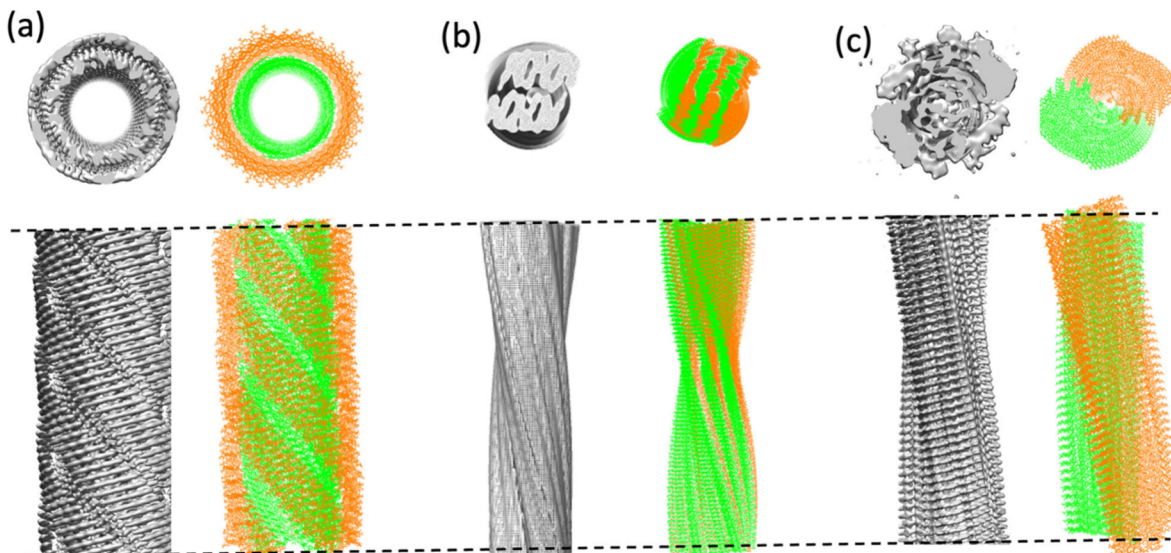


Figure 6. An overall morphological comparison between cryo-EM electron densities and FibrilGen-constructed atomistic models of cross- β nanostructures. (a) HP8 hydrogel tube: (left) electron density EMD-23487,¹⁸ (right) FibrilGen model structure. (b) AL1 rod: (left) electron density EMD-3128,⁴¹ (right) FibrilGen model structure. (c) $\text{A}\beta_{42}$ rod: (left) electron density EMD-3851,³⁴ (right) FibrilGen model structure. Electron densities visualized with Chimera 1.17.3.³⁰ FibrilGen models visualized with PyMOL.²⁷

later in the text and in Table S1. Using the Amber 19 molecular dynamics package,³¹ these peptides were modeled with the ff14SB force field³² in TIP3P water,³⁶ with added salt and additional Na^+ or Cl^- ions to neutralize the system (Table S1). Each simulation system was energy minimized and then heated to 100 K in the NVT ensemble for 20 ps; and then heated to 300 K in the NPT ensemble at a constant pressure of 1 bar for 400 ps. The system was then simulated at 300 K for a further 2 ns at a constant pressure of 1 bar. During the heating stages, the interatomic distances between central C_α atoms of consecutive β -strands (e.g., involving the fourth C_α atoms of 8-mer peptides) were constrained by flat-bottomed harmonic potentials for distances <2 Å and >9 Å using a force constant of 10 kcal/(mol Å²). Finally, the system was simulated for 1 μ s at 1 bar and 300 K. Simulations were conducted using a timestep of 4 fs via the hydrogen mass repartitioning (HMR)³⁷ methodology, where 2 amu was repartitioned from heavy atoms to hydrogens via the Amber *parmed* utility. A Langevin thermostat³⁸ with a collision frequency of 1 ps⁻¹ was employed and a Berendsen barostat³⁹ with a pressure relaxation time of 2 ps. Short-range nonbonded interactions used a cutoff distance of 10 Å and long-range electrostatic interactions were treated using the particle-mesh Ewald method.⁴⁰ Using a FibrilGen/MD workflow (Figure S12), we collected and analyzed the hypothetical cross- β structures. Hydrogen bonds over the peptide backbones are analyzed and counted, where the average backbone hydrogen bonds per peptide strand is reported. Here we evaluate a hydrogen bond as having an angle greater than 135° and distance between the nitrogen and the oxygen atoms of less than 3.5 Å. For analysis of the similarity between two cross- β nanostructures, we evaluate the root-mean-square deviation (RMSD) in C_α atom pair distances after alignment. For this alignment, the two sets of C_α coordinates \mathbf{C}_1 and \mathbf{C}_2 are translated to their centers of mass, represented as \mathbf{C}_{t1} and \mathbf{C}_{t2} . Then, \mathbf{C}_{t2} is rotated to \mathbf{C}_{r2} by an orthogonal matrix $\mathbf{R} = \mathbf{U}\mathbf{V}$, obtained from a singular vector decomposition $\mathbf{USV} = \mathbf{C}_{t1}\mathbf{C}_{t2}^T(\mathbf{C}_{t2}\mathbf{C}_{t2}^T)^{-1}$.

The fibril radius for a cross- β structure, R_β is calculated from the mean individual peptide centers of mass to the fibril long axis. Such a fibril long axis is fitted as described below. The periodic shift of peptides along the fibril long axis is represented by a vector \mathbf{v} , such that the fibril long axis $(\mathbf{O}^T, \mathbf{v}^T)^T$ represents the vector \mathbf{v} passing through a midpoint \mathbf{O} . The intrasheet peptide arrangement along the fibril long axis is represented by $(1, \mathbf{p}) (\mathbf{O}^T, \mathbf{v}^T)^T$, in such a way for \mathbf{p} , an integer vector of the numbering of peptides in each β -sheet, to scale the fibril long axis (Supporting Information, Figure S1). A linear regression model of mapping the fibril scaling $(1, \mathbf{p}) (\mathbf{O}^T, \mathbf{v}^T)^T$ to the peptide center of mass \mathbf{P} obtains an analytical solution of the fibril axis $(\mathbf{O}^T, \mathbf{v}^T)^T$ by $((1, \mathbf{p})^T(1, \mathbf{p}))^{-1}(1, \mathbf{p})^T\mathbf{P}$.

The relative orientation of two peptides g and $g-2$ within a β -sheet in the nanostructures was evaluated as follows: two C_α atoms i and j within peptide $g-2$ and one C_α atom i in peptide g were used to construct a local coordinate system ref- $i-j-i$ centered on the peptide $g-2$ $C_{\alpha,i}$ atom (Figure S2a); this was generated using vector x' in peptide $g-2$, from atom $C_{\alpha,i}$ to $C_{\alpha,j}$; and vector t from peptide g atom $C_{\alpha,i}$ to peptide $g-2$ atom $C_{\alpha,j}$. Here, we choose a linear segment of each peptide g and $g-2$; from this segment we assign the head and the tail C_α atoms as atom i and j , respectively. However, we note that the choice of i and j can be user-defined. Based on this coordinate system, we evaluate the orientation of peptide g relative to $g-2$: the backbone displacement along the local x -axis, termed the x -register, is represented by the x coordinate of vector t , t_x , for the peptide g $C_{\alpha,i}$ atom (Figure S2b). The backbone twisting in the local xz -plane, termed y -twisting, is represented by a twist angle $\theta_d = \tan^{-1}(d_z/d_x)$, where d is a vector in peptide g from $C_{\alpha,i}$ to $C_{\alpha,j}$ (Figure S2b).

3. RESULTS

3.1. Reconstruction of Atomistic Models. The FibrilGen library can be used to build and visualize in PyMol²⁷ a range of diverse cross- β nanostructure architectures (Figures S9–S11). As an example of the ability of FibrilGen to construct such systems at the atomic level, we generate models

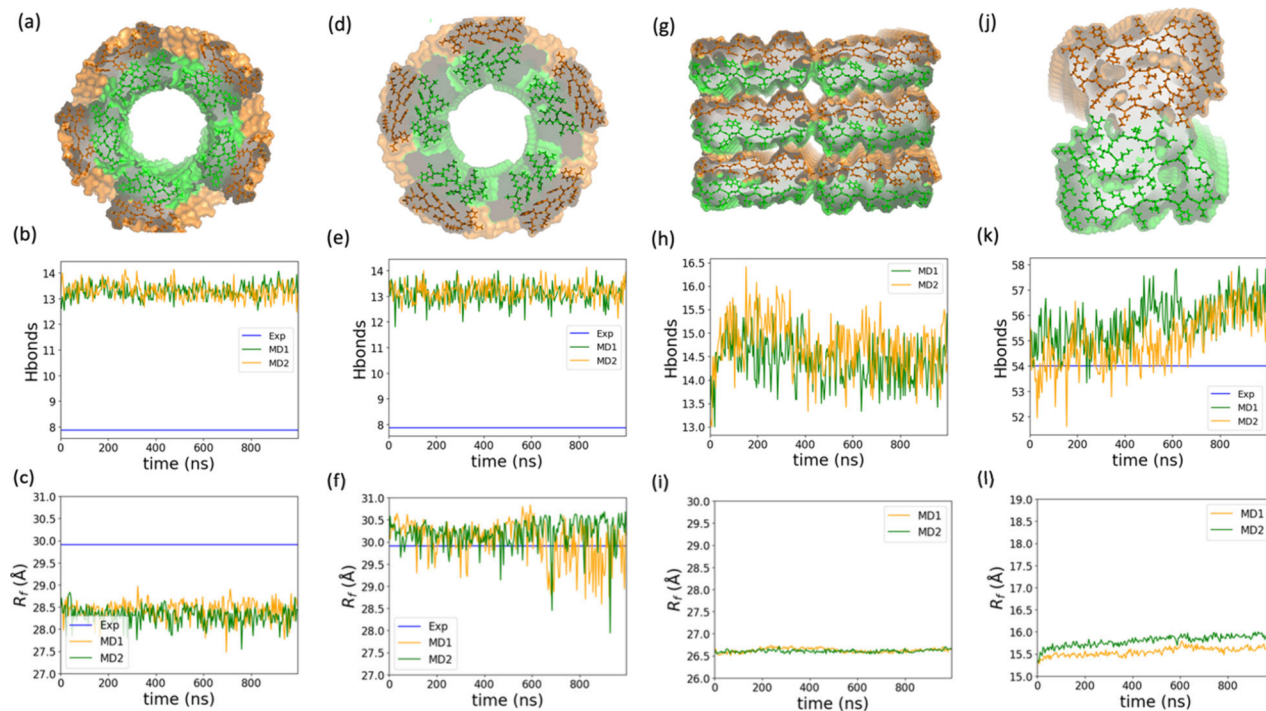


Figure 7. Generated (reconstructed) structure, the average backbone hydrogen bonds/strand (Hbonds), and fibril radius R_f during 1 μ s MD simulations at 300 K. Structures before equilibrations are (a) HP8 tube built by FibrilGen, (d) HP8 tube from cryo-EM structure 7LQI, (g) AL1 rod built by FibrilGen, and (j) $\text{A}\beta_{42}$ rod built by FibrilGen. Number of hydrogen bonds/strand (b, e, h, k), and fibril radius (c, f, i, l) calculated from MD replicates (yellow, green) are listed in the second and the third rows, respectively. Also shown is the baseline value calculated from the cryo-EM structure 7LQI (blue in b,c,e,f) and the cryo-EM structure SOQV (blue in k).

to compare with three experimentally determined cross- β structures of a differing morphology.

The first system is formed by Ac-FKFEFKFE-NH₂ peptides, denoted HP8 peptides, which assemble into a 10-sheet hydrogel tube.¹⁸ The tube is composed of parallel β -sheets in the inner wall and antiparallel β -sheets in the outer wall, as determined by cryo-EM to a resolution of 3.2 Å (Figure 6a). To construct an HP8 tube via FibrilGen, we first require a 2 × 2 peptide building block. As described in Methods, using a single peptide in a β -strand conformation as input, we employed *pep2unit* to generate a 2 × 2 unit where a parallel β -sheet and an antiparallel β -sheet are face-to-face aligned; five of these units were then built into a fibril model with 10 peptides in each sheet via FibrilGen, and energy minimized in explicit water using Amber. After this step, the central 2 × 2 unit was extracted and used to construct a new 10-sheet nanostructure, again of 10 peptides in a sheet (100 peptides in total). We use FibrilGen to explore tilt angle values (15°, 20°, 25°, 30°, 35°) for this tube assembly and we found that after the internal refinement in FibrilGen (Section 2.4), the helical twists converge to a tilt angle θ_z of 25.0° and a twist angle θ_y of 3.7°. This geometry agrees well with the respective values of 30.0° and 4.5° for the observed HP8 nanostructure (Figure 6a); these estimates were obtained on fitting of a helical model to the reconstructed cryo-EM structure (see Supporting Information for details).

The second system is comprised of IGSNVVTWYQQQL self-assembling β -peptides, denoted AL1, which are observed to form a 12-sheet rod nanostructure of cryo-EM reconstructed at 8.3 Å resolution (Figure 6b).²⁸ It is composed of parallel β -sheets, as confirmed by ssNMR.²⁸ To generate an AL1 rod, a constituent β -strand peptide was first built and then assembled

with *pep2unit* into a 2 × 2 unit, featuring two parallel β -sheets in a face-to-face alignment. Based on the energy minimized unit, a collection of initial tilt angles (3°, 5°, 7°, 9°, 10°) were explored for building and refining the two-sheet 192-peptide rod geometry. Different from the HP8 tube, FibrilGen suggests a range of helical twists are sterically allowed for the AL1 rod, including a helical morphology with a tilt angle θ_z of 11.0° and a twist angle θ_y of 1.5°. These values closely resemble the model reconstructed from cryo-EM electron density (Figure 6b), which has a tilt angle θ_z of 12.2° and a twist angle θ_y of 1.4°.

The third system considered is formed by $\text{A}\beta_{42}$, amyloid- β peptides which assemble into a two-sheet rod, as determined by ssNMR³⁴ and by cryo-EM³⁴ to 4.0 Å resolution (Figure 6c). To build a $\text{A}\beta_{42}$ rod with FibrilGen, instead of using *pep2unit*, we took the 2 × 2 unit from the cryo-EM structure (PDB code SOQV) as a unit, without energy minimization in Amber. Then to build a 2-sheet fibril of 44 peptides, we initialized a range of initial tilt angles (3°, 5°, 7°, 9°, 10°) to build and refine the rod morphology. Different from the AL1 rod, the adjusted twists converge to a tilt angle θ_z of 3.5° and a twist angle θ_y of 1.0°; this is close to the values of 4.5° and 1.4° respectively derived from the experimental structure of $\text{A}\beta_{42}$ rod (Figure 6c).

3.2. Assessment of Structural Stability. Here, we evaluated the structural stability of the FibrilGen generated atomistic structures of HP8, AL1 and $\text{A}\beta_{42}$, and a cryo-EM structure of HP8 (pdb: 7LQI) in water via molecular dynamics simulations. Two replicas of a 1 μ s MD simulation were performed at 300 K.

HP8 Tube. For the MD simulation of the FibrilGen-constructed 10-sheet HP8 tube, the RMSD in C_α atoms for the

Table 2. Time Averaged Structural Properties of Cross- β Nanostructures from Microsecond MD Simulations (final 400 ns), for FibrilGen-Constructed HP8 Tube, AL1 Rod, and $\text{A}\beta_{42}$ Rod, and for Cryo-EM Structure of HP8 Tube Averaged over Two Replicates^a

Cross- β structures	Peptide register t_x (\AA)	Peptide twist θ_d (deg)	Fibril radius R_f (\AA)	Hydrogen bonds/strand
HP8 tube ^b	7.1 ± 0.3	14.3 ± 2.1	28.3 ± 0.2	13.2 ± 0.3
HP8 tube ^c	7.0 ± 0.3	19.1 ± 3.3	30.0 ± 0.5	13.1 ± 0.3
HP8 cryo-EM ^d	6.4	13.0	30.0	7.8
AL1 rod ^b	0.0 ± 0.2	3.7 ± 1.0	26.6 ± 0.0	14.4 ± 0.4
$\text{A}\beta_{42}$ rod ^b	-0.1 ± 0.3	7.0 ± 3.9	15.7 ± 0.1	56.1 ± 0.7
$\text{A}\beta_{42}$ cryo-EM ^e	0.2	2.5	N/A	54.0

^aValues for cryo-EM structures of HP8 (PDB code 7LQI) and $\text{A}\beta_{42}$ (PDB code 5OQV) also shown. ^bMD initiated from FibrilGen-generated structure. ^cMD initiated from cryo-EM structure PDB code 7LQI. ^dCryo-EM structure PDB code 7LQI. ^eCryo-EM structure PDB code 5OQV.

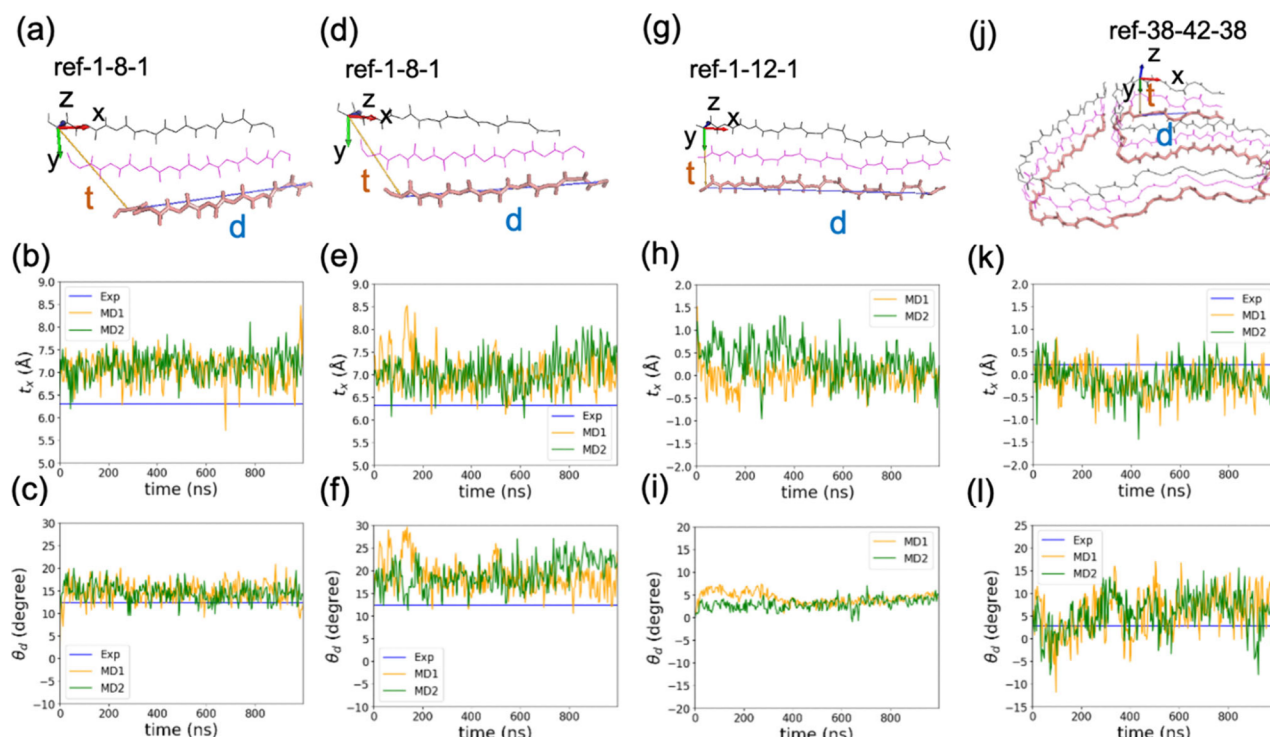


Figure 8. Time series for relative peptide alignment (x -register t_x , y -twist angle θ_d) over replicate microsecond MD simulations at 300 K (yellow, green) for (a–c) an HP8 tube built by FibrilGen, (d–f) an HP8 tube from cryo-EM structure 7LQI, (g–i) an AL1 rod built by FibrilGen, and (j–l) an $\text{A}\beta_{42}$ rod built by FibrilGen. Experimental values indicated in blue. Local coordinate systems to define t_x and θ_d for the four systems shown in (a), (d), (g), and (j). A baseline peptide alignment calculated from the cryo-EM structure 7LQI (blue in b,c,e,f) and the cryo-EM structure 5OQV (blue in k,l).

two replicas converge to values of 2.8 and 3.3 \AA from the FibrilGen structure (Figure S3a,b), suggesting that these nanostructures occupy a stable well on their free energy surface. Relative to cryo-EM structure 7LQI, these replicas converge to C_α RMSD values of 2.5 and 3.0 \AA respectively (Figure S4a), similar to the value of 1.97 \AA found for the initial FibrilGen model. Inspection of snapshot structures from these trajectories further confirms that the constructed tube morphology of HP8 is maintained over the microsecond simulations and resembles both the initial FibrilGen and cryo-EM structure. Additionally, two replicate microsecond MD simulations were initiated from this cryo-EM structure of HP8. Relative to its initial cryo-EM structure, the trajectories exhibited converged C_α RMSDs of 1.7 and 2.0 \AA over the final 400 ns of the trajectory (Figure S3c,d).

We also quantify overall structural properties of the HP8 tube (Figure 7a) by computing the backbone hydrogen bonds, fibril radius R_f and the relative orientation of stacking peptides

via average x -register t_x and twist angle θ_d (see Section 2.5). In the replicate simulations of the FibrilGen-built HP8 nanostructure, hydrogen bonds formed by the second to the ninth amino acid residues (the first and the tenth are terminal caps) were well populated (Figure S8c), compared to the cryo-EM structure 7LQI before (Figure S8a) and after MD simulation (Figure S8b). Over MD simulation, the HP8 tube had an average backbone hydrogen bond number per strand of 13.2 ± 0.3 (Figure 7b, Table 2), similar to the cryo-EM structure that had an average backbone hydrogen bond number of 13.1 ± 0.3 (Figure 7e, Table 2). Furthermore, the HP8 tube adopts a stable radius, with a R_f value of $28.3 \pm 0.2 \text{\AA}$ averaged over the two trajectories (Figure 7c, Table 2, Table S2). This mean value is slightly narrower than the radius in the cryo-EM structure of 30 \AA ; this radius is maintained in the MD simulations from the cryo-EM structure with a mean value of $30.0 \pm 0.5 \text{\AA}$ over the microsecond simulations (Figure 7f, Table 2). Regarding the relative alignment of neighboring

peptides in the outer wall β -sheet of HP8 (Figure 8a), in the replicate FibrilGen model simulations of HP8, we observe an average x-register t_x of 7.1 ± 0.3 Å (Figure 8b), and a left-handed twist angle θ_d of $14.3 \pm 2.1^\circ$ (Figure 8c). This alignment compares well with the cryo-EM structure (Figure 7d), which has a t_x value of 6.4 Å and a θ_d angle of 13° . MD simulation from the cryo-EM structure finds similar values of t_x and θ_d , with respective values of 7.0 ± 0.3 Å and $19.1 \pm 3.3^\circ$ (Figure 8e,f). In conclusion, the FibrilGen model produces an atomistic model that is stable under simulation at 300 K and that compares well with a reconstructed model from cryo-EM and its simulation.

AL1 Rod. Starting from the FibrilGen structure of the 12-sheet 192-peptide AL1 rod (Figure 7g), replicate microsecond MD trajectories converge to C_α RMSD values of 3.4 Å in both cases (Figure S3e,f). The backbone hydrogen bonds were well populated by the fourth to tenth amino acids (Figure S8e). Over the MD trajectories, the number backbone hydrogen bonds per strand converged to 14.5 (Figure 7h) and the average was 14.4 ± 0.4 over the last 400 ns (Table 2). The overall morphology of the simulated AL1 rod is maintained with a persistent fibril radius of 26.6 Å (Figure 7i). Within the outer wall β -sheet of AL1, we compute an average x-register t_x of 0.0 ± 0.2 Å and a left-handed twist θ_d of $3.7 \pm 1.0^\circ$ (Figure 8h,i, Table 2). While no atomistic model for AL1 is available from experiment, the stable twisted rod-like nanostructure obtained from MD appears to be consistent with the observed electron density observed from cryo-EM.²⁸ In this work,²⁸ the alignment of AL1 peptides was further confirmed by magic angle spinning (MAS) solid state NMR (ssNMR) spectroscopy of isotopically labeled AL1 peptides. Interpretation of the AL1 backbone conformation indicated an in-register alignment of β -strands and a left-handed twist. These observations are consistent with the t_x and θ_d values we obtained from our simulated model above.

$\text{A}\beta_{42}$ Rod. Replicate molecular simulations of the two-sheet 44-peptide $\text{A}\beta_{42}$ nanostructure built by FibrilGen (Figure 7j) were performed. The replicates converge in both cases to a C_α RMSD value of 2.4 Å from the FibrilGen model (Figure S3g,h). This corresponds to a C_α RMSD value of 1.4 Å from the cryo-EM structure 5OQV³⁴ (Figure S4b), starting from an initial value of 0.7 Å. Given that there were five turns on the $\text{A}\beta_{42}$ monomer, some intrasheet backbone hydrogen bonds were not strong and would not be counted in our hydrogen bond calculations. Over the MD simulations, we observe an average number of backbone hydrogen bonds of 56.1 ± 0.7 , similar to the cryo-EM structure that had 54 backbone hydrogen bonds (Figure 7k, Table 2). In terms of morphology, we observe an average fibril radius R_f value of 15.7 ± 0.1 Å, computed over the last 400 ns of the combined trajectories (Figure 7k,l, Table 2). The relative peptide orientation in the β -sheets exhibits an x-register t_x of -0.1 ± 0.3 Å (Figure 8k). This near zero x-register value corresponds to an in-register backbone alignment and agrees with ssNMR observations.³⁴ We also note that the simulated left-handed twist angle θ_d of $7.0 \pm 3.9^\circ$ (Figure 8l) is not significantly different from the experimental cryo-EM³⁴ value from of a left-handed twist θ_d of 3° .

3.3. Assessment of Hypothetical Structures. In the preceding work, we have used a modeling/MD workflow to assess the stability of experimentally observed morphologies for a given peptide system. In order to probe the ability of this workflow to assess other potentially less favorable morpholo-

gies that are not observed experimentally, we exchanged the morphologies of HP8 and AL1 systems, such that the HP8 tube was modeled as a HP8 rod, and the AL1 rod was modeled as a AL1 tube. FibrilGen was used to generate HP8 rod and AL1 tube structures (Table S1).

Specifically, for HP8, two parallel β -sheets in $\beta_p\alpha\beta_p$ alignment (Figure 3d) were built by *pep2unit*; this two-sheet structure was energy minimized, and then a 2×2 peptide unit was selected from it as a building block from which to assemble a 12-sheet rod as the AL1 nanostructure (following the approach detailed in Sections 2.2–2.4). A rod of net positively charged HP8 (all glutamate residues protonated as per pH 3) and a rod of net neutral HP8 (all glutamate residues deprotonated consistent with pH 7) were built to compared with the positively charged HP8 tube (HP8 in the inner shell was neutral, and HP8 in the outer shell was positively charged in accord with pH 4). Both rod structures were modeled in explicit solvent (Table S1) to be energy minimized and equilibrated (Section 2.5). The positively charged HP8 rod could be energy minimized but dissociated during equilibration (Figure S5a). The neutral HP8 rod kept its overall assembly, and during replicate 1 μ s production simulations the morphology converged into a staggered arrangement (Figure S5b), with an average number of backbone hydrogen bonds of 11.0 ± 0.6 , peptide register t_x of 0.0 ± 0.2 Å, peptide twist θ_d of $0.2 \pm 2.2^\circ$, and fibril radius R_f of 25.7 ± 0.1 Å (Table 3, Figure

Table 3. Morphology Swapping of HP8 and AL1 and Structural Properties Averaged over Final 400 ns of Replicate Microsecond MD Simulations^a

Cross- β structures	Peptide register t_x (Å)	Peptide twist θ_d (deg)	Fibril radius R_f (Å)	Hydrogen bonds/strand
HP8 rod (charged)	n/s	n/s	n/s	n/s
HP8 rod (neutral)	0.0 ± 0.2	0.2 ± 2.2	25.7 ± 0.1	11.0 ± 0.6
AL1 tube	n/s	n/s	n/s	n/s
AL1 sheet x2	1.3 ± 0.3	0.6 ± 1.4	4.9 ± 0.0	13.6 ± 0.3

^an/s indicates not stable.

S7a–d). The HP8 system made fewer backbone hydrogen bonds per strand in this rod morphology compared with the HP8 tube arrangement (Figure S8d and c), with values of 11.0 and 13.2, respectively (Tables 3 and 2). Also, when compared to the AL1 rod, which had a peptide twist of 3.7° (Table 2), the neutral HP8 rod adopted a flatter conformation, where the twist between neighboring peptides reduced to 0.2° (Table 3).

A similar protocol for assembling an AL1 tube was followed, where the AL1 peptides were assembled into a 2×2 unit that combined a parallel and an antiparallel sheet ($\beta_p\alpha\beta_a$, Figure S6) as in the HP8 tube. However, an energy minimization of such 2×2 units led to ruptured backbone hydrogen bonds and significant loss of β -sheet conformation. Consequently, we instead used the 2×2 unit in the AL1 rod and investigated the feasible fibril structures into which it could assemble. This 2×2 unit, however, was not viable to assemble into tube and ribbon morphologies with rotational stacking of 2, 3, 4, and 5 repeats (Figure S6a). To construct an AL1 fibril structure assembled with a rotational stacking, we took two flat sheets and aligned them face-to-face (Figure S6c). This AL1 sheet structure could be energy minimized and equilibrated and also proved to be stable in the replicate production simulations

(Figure S6c, Figure S7e and f), with an average backbone hydrogen bonds of 13.6 ± 0.3 , a peptide register t_x of 1.3 ± 0.3 Å, a peptide twist θ_q of $0.6 \pm 1.4^\circ$, and a fibril radius R_f of 4.9 ± 0.0 Å (Table 3). This twist value was significantly lower than that of the AL1 rod value of 3.7° and the HP8 tube value of 14.3° . Compared to AL1 rod, AL1 sheet had slightly less backbone hydrogen bonds from the fourth to the tenth amino acids (Figure S8e and f). The overall AL1 sheet made 0.8 fewer backbone hydrogen bonds on average than the AL1 rod, with respective values of 13.6 ± 0.3 and 14.4 ± 0.4 (Tables 3 and 2).

Therefore, in this section, we have constructed, simulated, and analyzed hypothetical HP8 and AL1 fibril morphologies. Given the same modeling pipeline, alternative peptide assemblies were built and compared with the corresponding experimentally observed peptide assemblies. We found that some arrangement of peptide assemblies (e.g., AL1 tubes and a positively charged HP8 rod) were rejected in the energy minimization of the 2×2 unit assembly, geometrical arrangement in FibrilGen, or the structural refinement in water. Furthermore, we found some nonexperimental peptide assemblies (e.g., the neutral HP8 rod and AL1 sheet) that were not rejected from the FibrilGen/MD workflow. These structures did appear to exhibit slightly less backbone hydrogen bonding which could be indicative of being not as favorable as the experimentally observed structures.

4. DISCUSSION AND CONCLUSIONS

In this work, we introduce a Python library called FibrilGen to model cross- β nanofibrils in diverse morphologies. The package allows users to generate atomistic cross- β nanostructures in flat sheets and a broad range of rods, ribbons, and tubes, with automatic refinement to ensure the helical structures are compact without steric clashes. FibrilGen is compatible with PyMOL so that the user can conveniently invoke FibrilGen functions at the PyMOL command line to build and visualize in PyMOL the resulting generated cross- β structures.

To exemplify its ability to construct realistic cross- β structures, we assessed the use of FibrilGen to generate atomistic cross- β structures comparable to experimental data for three peptide systems, HP8, AL1 and $\text{A}\beta_{42}$, that form rods and tubes. We find good agreement with the available experimental data for FibrilGen-built cross- β nanostructures of these peptide assemblies. Furthermore, these realistic cross- β nanostructure morphologies provide input coordinates to MD simulation; the peptide assemblies are stable when simulated on the microsecond time scale at 300 K and also yield average geometric parameters in good agreement with helical 3D models reconstructed from experiment.

To then explore the ability of the FibrilGen modeling workflow to identify favored nanofibril arrangements, we assessed a HP8 rod and an AL1 tube that have not been experimentally observed in cryo-EM structures. For HP8, we considered two different charge states of the peptide: (i) net positive peptides with all glutamate residues protonated and (ii) net neutral peptides with all glutamates ionized. Interestingly, we found that the charged HP8 rod collapsed during the MD equilibration. The neutral HP8 rod was able to form a stable assembly during equilibration and production simulations, but in the rod structure, the peptide backbone made fewer hydrogen bonds than in the tube structure. For AL1 modeled in a tube morphology, sterically allowed

structures were not found. Here, an AL1 sheet morphology was possible but again exhibited fewer backbone hydrogen bonds than the rod structure. These observations do align with experimental observations that suggest an HP8 tube rather than an HP8 rod is favored and an AL1 rod rather than an AL1 tube. However, we note that ideally the predicted free energy of likely morphologies should be used to guide the assessment of stability, although computation of this for large complex nanostructures is challenging and will be a focus of future work.

The application of this FibrilGen/MD workflow provides a means to readily generate a potential fibril assembly for a given peptide. Indeed, some peptides can form multiple cross- β morphologies that coexist under the same conditions.²⁸ For peptides of arbitrary sequence, one could envisage exploring a variety of assemblies according to input parameters (Figure 2). The FibrilGen structures could be modeled with guidance from available cryo-EM and ssNMR information, or could be purely hypothetical. Some of these structures might prove sterically incompatible in FibrilGen or unstable in subsequent MD simulation, as was the case for the AL1 system, where various arrangements such as a tube were found to be disfavored (Figure S6). One could also conceive constructing initial fibril models for an arbitrary peptide sequence (akin to Figures S10 and S11), with subsequent simulation and computational site directed mutagenesis to further assess stability. An interesting application in this regard, given in particular FibrilGen's use of helical twist as a coordinate to optimize steric effects, could be modeling the effect on predicted nanostructure morphology and supramolecular chirality of peptide side-chain identity. For example, recent experimental work has determined that the twist of the β -sheet changes from left-handed to right-handed as alanines are replaced by valines in a series of peptide amphiphiles.⁴² The FibrilGen/MD workflow offers a feasible route to model diverse β -sheet nanofibril structures, which are not as readily accessible via assembly programs such as PACKMOL, Nanomaterial Modeler, PolyPly, or via empirical inference from AlphaFold⁴³ and Rosetta⁴⁴ models. Systematic exploration of the potentially packing and twist of β -sheet nanofibrils using the FibrilGen/MD workflow could aid the design of β -peptides that combine to form novel biomaterials, fibril networks,⁴⁵ and drug delivery vehicles.

■ ASSOCIATED CONTENT

Data Availability Statement

The source code is available on GitHub at <https://github.com/ChaoYuYang0/FibrilGen-v0.git> and as a .zip file in Supporting Information. Documentation is provided in README; example scripts for fibril generation are provided in scripts/; an implementation of fitting the long axis of a fibril structure is provided in analysis/; and FibrilGen structures shown in this paper are provided in structures/output/.

SI Supporting Information

The Supporting Information is available free of charge at <https://pubs.acs.org/doi/10.1021/acs.jcim.5c02108>.

Details of simulation systems, structural analyses and examples of FibrilGen usage (PDF). Two variants of FibrilGen code are provided: the first .zip file is compatible for newer PyMOL versions, and the second one is compatible for older PyMOL versions. Detailed

information can be found in the respective folder README files.

FibrilGen code is compatible for newer PyMOL versions ([ZIP](#))

FibrilGen code is compatible for older PyMOL versions ([ZIP](#))

AUTHOR INFORMATION

Corresponding Author

Richard A. Bryce — *Division of Pharmacy and Optometry, School of Health Sciences, Faculty of Biology, Medicine and Health, The University of Manchester, Manchester M13 9PL, United Kingdom; [orcid.org/0000-0002-8145-2345](#); Phone: (0)161-275-8345; Email: R.A.Bryce@manchester.ac.uk; Fax: (0)161-275-2481*

Authors

Chao-Yu Yang — *Department of Materials, Manchester Institute of Biotechnology, School of Natural Sciences, Faculty of Science and Engineering, The University of Manchester, Manchester M13 9PL, United Kingdom*

Aline F. Miller — *Department of Chemical Engineering, Manchester Institute of Biotechnology, School of Engineering, Faculty of Science and Engineering, The University of Manchester, Manchester M1 7DN, United Kingdom*

Alberto Saiani — *Division of Pharmacy and Optometry, Manchester Institute of Biotechnology, School of Health Sciences, Faculty of Biology, Medicine and Health, The University of Manchester, Manchester M13 9PL, United Kingdom; [orcid.org/0000-0002-5504-8306](#)*

Complete contact information is available at:

<https://pubs.acs.org/10.1021/acs.jcim.Sc02108>

Author Contributions

C.-Y.Y., A.S., and R.A.B. conceived the study. C.-Y.Y. designed and wrote the code and performed and analyzed the molecular dynamics simulations. R.A.B., A.F.M., and A.S. supervised the research. C.-Y.Y. drafted the manuscript. R.A.B. and A.S. edited and revised the manuscript.

Notes

The authors declare no competing financial interest.

ACKNOWLEDGMENTS

The authors would like to acknowledge the assistance given by Research IT and the use of the Computational Shared Facility at the University of Manchester.

REFERENCES

- (1) Gazit, E. Self-assembled peptide nanostructures: the design of molecular building blocks and their technological utilization. *Chem. Soc. Rev.* **2007**, *36* (8), 1263–9.
- (2) Ulijn, R. V.; Smith, A. M. Designing peptide based nanomaterials. *Chem. Soc. Rev.* **2008**, *37* (4), 664–75.
- (3) Hartgerink, J. D.; Beniash, E.; Stupp, S. I. Peptide-amphiphile nanofibers: a versatile scaffold for the preparation of self-assembling materials. *Proc. Natl. Acad. Sci. U. S. A.* **2002**, *99* (8), 5133–8.
- (4) Lee, N. R.; Bowerman, C. J.; Nilsson, B. L. Effects of varied sequence pattern on the self-assembly of amphipathic peptides. *Biomacromolecules* **2013**, *14* (9), 3267–77.
- (5) Bowerman, C. J.; Liyanage, W.; Federation, A. J.; Nilsson, B. L. Tuning beta-sheet peptide self-assembly and hydrogelation behavior by modification of sequence hydrophobicity and aromaticity. *Biomacromolecules* **2011**, *12* (7), 2735–45.

(6) Boothroyd, S.; Miller, A. F.; Saiani, A. From fibres to networks using self-assembling peptides. *Faraday Discuss.* **2013**, *166*, 195–207.

(7) Sinha, N. J.; Langenstein, M. G.; Pochan, D. J.; Kloxin, C. J.; Saven, J. G. Peptide Design and Self-assembly into Targeted Nanostructure and Functional Materials. *Chem. Rev.* **2021**, *121* (22), 13915–13935.

(8) Sheehan, F.; Sementa, D.; Jain, A.; Kumar, M.; Tayarani-Najjaran, M.; Kroiss, D.; Ulijn, R. V. Peptide-Based Supramolecular Systems Chemistry. *Chem. Rev.* **2021**, *121* (22), 13869–13914.

(9) Wang, F.; Gnewou, O.; Solemanifar, A.; Conticello, V. P.; Egelman, E. H. Cryo-EM of Helical Polymers. *Chem. Rev.* **2022**, *122* (17), 14055–14065.

(10) Caliari, S. R.; Burdick, J. A. A practical guide to hydrogels for cell culture. *Nat. Methods* **2016**, *13* (5), 405–14.

(11) Elsawy, M. A.; Wychowaniec, J. K.; Castillo Diaz, L. A.; Smith, A. M.; Miller, A. F.; Saiani, A. Controlling Doxorubicin Release from a Peptide Hydrogel through Fine-Tuning of Drug-Peptide Fiber Interactions. *Biomacromolecules* **2022**, *23* (6), 2624–2634.

(12) Revete, A.; Aparicio, A.; Cisterna, B. A.; Revete, J.; Luis, L.; Ibarra, E.; Segura Gonzalez, E. A.; Molino, J.; Reginensi, D. Advancements in the Use of Hydrogels for Regenerative Medicine: Properties and Biomedical Applications. *Int. J. Biomater.* **2022**, *2022*, 3606765.

(13) Lu, P.; Ruan, D.; Huang, M.; Tian, M.; Zhu, K.; Gan, Z.; Xiao, Z. Harnessing the potential of hydrogels for advanced therapeutic applications: current achievements and future directions. *Signal Transduct Target Ther.* **2024**, *9* (1), 166.

(14) Du, Z.; Fan, B.; Dai, Q.; Wang, L.; Guo, J.; Ye, Z.; Cui, N.; Chen, J.; Tan, K.; Li, R.; Tang, W. Supramolecular peptide nanostructures: Self-assembly and biomedical applications. *Giant* **2022**, *9*, 100082.

(15) Eisenberg, D. S.; Sawaya, M. R. Structural Studies of Amyloid Proteins at the Molecular Level. *Annu. Rev. Biochem.* **2017**, *86*, 69–95.

(16) Sawaya, M. R.; Sambashivan, S.; Nelson, R.; Ivanova, M. I.; Sievers, S. A.; Apostol, M. I.; Thompson, M. J.; Balbirnie, M.; Wiltzius, J. J.; McFarlane, H. T.; Madsen, A. O.; Riek, C.; Eisenberg, D. Atomic structures of amyloid cross-beta spines reveal varied steric zippers. *Nature* **2007**, *447* (7143), 453–7.

(17) Petkova, A. T.; Ishii, Y.; Balbach, J. J.; Antzutkin, O. N.; Leapman, R. D.; Delaglio, F.; Tycko, R. A structural model for Alzheimer's beta -amyloid fibrils based on experimental constraints from solid state NMR. *Proc. Natl. Acad. Sci. U. S. A.* **2002**, *99* (26), 16742–7.

(18) Wang, F.; Gnewou, O.; Wang, S.; Osinski, T.; Zuo, X.; Egelman, E. H.; Conticello, V. P. Deterministic chaos in the self-assembly of beta sheet nanotubes from an amphipathic oligopeptide. *Matter* **2021**, *4* (10), 3217–3231.

(19) Soliman, M. A. N.; Khedr, A.; Sahota, T.; Armitage, R.; Allan, R.; Laird, K.; Alcock, N.; Ghouloum, F. I.; Amer, M. H.; Alazragi, R.; Edwards-Gayle, C. J. C.; Wychowaniec, J. K.; Vargiu, A. V.; Elsawy, M. A. Unraveling the Atomistic Mechanism of Electrostatic Lateral Association of Peptide beta-Sheet Structures and Its Role in Nanofiber Growth and Hydrogelation. *Small* **2025**, *21* (6), No. e2408213.

(20) Scheres, S. H. RELION: implementation of a Bayesian approach to cryo-EM structure determination. *J. Struct Biol.* **2012**, *180* (3), 519–30.

(21) Leaver-Fay, A.; Tyka, M.; Lewis, S. M.; Lange, O. F.; Thompson, J.; Jacak, R.; Kaufman, K.; Renfrew, P. D.; Smith, C. A.; Sheffler, W.; Davis, I. W.; Cooper, S.; Treuille, A.; Mandell, D. J.; Richter, F.; Ban, Y. E.; Fleishman, S. J.; Corn, J. E.; Kim, D. E.; Lyskov, S.; Berrondo, M.; Mentzer, S.; Popovic, Z.; Havranek, J. J.; Karanicolas, J.; Das, R.; Meiler, J.; Kortemme, T.; Gray, J. J.; Kuhlman, B.; Baker, D.; Bradley, P. ROSETTA3: an object-oriented software suite for the simulation and design of macromolecules. *Methods Enzymol* **2011**, *487*, 545–74.

(22) Adams, P. D.; Afonine, P. V.; Bunkoczi, G.; Chen, V. B.; Davis, I. W.; Echols, N.; Headd, J. J.; Hung, L. W.; Kapral, G. J.; Gross-Kunstleve, R. W.; McCoy, A. J.; Moriarty, N. W.; Oeffner, R.; Read, R.

- J.; Richardson, D. C.; Richardson, J. S.; Terwilliger, T. C.; Zwart, P. H. PHENIX: a comprehensive Python-based system for macromolecular structure solution. *Acta Crystallogr. D Biol. Crystallogr.* **2010**, *66*, 213–21.
- (23) Trabuco, L. G.; Villa, E.; Schreiner, E.; Harrison, C. B.; Schulten, K. Molecular dynamics flexible fitting: a practical guide to combine cryo-electron microscopy and X-ray crystallography. *Methods* **2009**, *49* (2), 174–80.
- (24) Martinez, L.; Andrade, R.; Birgin, E. G.; Martinez, J. M. PACKMOL: a package for building initial configurations for molecular dynamics simulations. *J. Comput. Chem.* **2009**, *30* (13), 2157–64.
- (25) Grunewald, F.; Alessandri, R.; Kroon, P. C.; Monticelli, L.; Souza, P. C. T.; Marrink, S. J. PolyPy; a python suite for facilitating simulations of macromolecules and nanomaterials. *Nat. Commun.* **2022**, *13* (1), 68.
- (26) Choi, Y. K.; Kern, N. R.; Kim, S.; Kanhaiya, K.; Afshar, Y.; Jeon, S. H.; Jo, S.; Brooks, B. R.; Lee, J.; Tadmor, E. B.; Heinz, H.; Im, W. CHARMM-GUI Nanomaterial Modeler for Modeling and Simulation of Nanomaterial Systems. *J. Chem. Theory Comput.* **2022**, *18* (1), 479–493.
- (27) *The PyMOL Molecular Graphics System*, Version 1.8, Schrodinger, LLC, 2015.
- (28) Close, W.; Neumann, M.; Schmidt, A.; Hora, M.; Annamalai, K.; Schmidt, M.; Reif, B.; Schmidt, V.; Grigorieff, N.; Fandrich, M. Physical basis of amyloid fibril polymorphism. *Nat. Commun.* **2018**, *9* (1), 699.
- (29) Fitzpatrick, A. W.; Debelouchina, G. T.; Bayro, M. J.; Clare, D. K.; Caporini, M. A.; Bajaj, V. S.; Jaroniec, C. P.; Wang, L.; Ladizhansky, V.; Muller, S. A.; MacPhee, C. E.; Waudby, C. A.; Mott, H. R.; De Simone, A.; Knowles, T. P.; Saibil, H. R.; Vendruscolo, M.; Orlova, E. V.; Griffin, R. G.; Dobson, C. M. Atomic structure and hierarchical assembly of a cross-beta amyloid fibril. *Proc. Natl. Acad. Sci. U. S. A.* **2013**, *110* (14), 5468–73.
- (30) Pettersen, E. F.; Goddard, T. D.; Huang, C. C.; Couch, G. S.; Greenblatt, D. M.; Meng, E. C.; Ferrin, T. E. UCSF Chimera—a visualization system for exploratory research and analysis. *J. Comput. Chem.* **2004**, *25* (13), 1605–12.
- (31) Case, D. A.; Metin, A. H.; Belfon, K.; Ben-Shalom, I.; Brozell, S. R.; Cerutti, D. S.; Thomas; Cruzeiro, V. W. D. D.; T, A.; Duke, R. E. *Amber 2021*; University of California: San Francisco, 2021.
- (32) Maier, J. A.; Martinez, C.; Kasavajhala, K.; Wickstrom, L.; Hauser, K. E.; Simmerling, C. ff14SB: Improving the Accuracy of Protein Side Chain and Backbone Parameters from ff99SB. *J. Chem. Theory Comput.* **2015**, *11* (8), 3696–713.
- (33) Mark, P.; Nilsson, L. Structure and Dynamics of the TIP3P, SPC, and SPC/E Water Models at 298K. *J. Phys. Chem. A* **2001**, *105*, 9954–9960.
- (34) Gremer, L.; Scholzel, D.; Schenk, C.; Reinartz, E.; Labahn, J.; Ravelli, R. B. G.; Tusche, M.; Lopez-Iglesias, C.; Hoyer, W.; Heise, H.; Willbold, D.; Schroder, G. F. Fibril structure of amyloid-beta(1–42) by cryo-electron microscopy. *Science* **2017**, *358* (6359), 116–119.
- (35) Bruce, N. J.; Chen, D.; Dastidar, S. G.; Marks, G. E.; Schein, C. H.; Bryce, R. A. Molecular dynamics simulations of Abeta fibril interactions with beta-sheet breaker peptides. *Peptides* **2010**, *31* (11), 2100–8.
- (36) Jorgensen, W. L.; Chandrasekhar, J.; Madura, J. D.; Impey, R. W.; Klein, M. L. Comparison of simple potential functions for simulating liquid water. *J. Chem. Phys.* **1983**, *79*, 926–935.
- (37) Feenstra, K. A.; Hess, B.; Berendsen, H. J. C. Improving Efficiency of Large Time-Scale Molecular Dynamics Simulations of Hydrogen-Rich Systems. *J. Comput. Chem.* **1999**, *20*, 786–798.
- (38) Feller, S. E.; Zhang, Y.; Pastor, R. W.; Brooks, B. R. Constant pressure molecular dynamics simulation: The Langevin piston method. *J. Chem. Phys.* **1995**, *103* (11), 4613–4621.
- (39) Berendsen, H. J. C.; Postma, J. P. M.; van Gunsteren, W. F.; DiNola, A.; Haak, J. R. Molecular dynamics with coupling to an external bath. *J. Chem. Phys.* **1984**, *81* (8), 3684–3690.
- (40) Essmann, U.; Perera, L.; Berkowitz, M. L.; Darden, T.; Lee, H.; Pedersen, L. G. A smooth particle mesh Ewald method. *J. Chem. Phys.* **1995**, *103* (19), 8577–8593.
- (41) Schmidt, A.; Annamalai, K.; Schmidt, M.; Grigorieff, N.; Fandrich, M. Cryo-EM reveals the steric zipper structure of a light chain-derived amyloid fibril. *Proc. Natl. Acad. Sci. U. S. A.* **2016**, *113* (22), 6200–5.
- (42) Sangji, M. H.; Sai, H.; Chin, S. M.; Lee, S. R.; I, R. S.; Palmer, L. C.; Stupp, S. I. Supramolecular Interactions and Morphology of Self-Assembling Peptide Amphiphile Nanostructures. *Nano Lett.* **2021**, *21* (14), 6146–6155.
- (43) Abramson, J.; Adler, J.; Dunger, J.; Evans, R.; Green, T.; Pritzel, A.; Ronneberger, O.; Willmore, L.; Ballard, A. J.; Bambrick, J.; Bodenstein, S. W.; Evans, D. A.; Hung, C. C.; O'Neill, M.; Reiman, D.; Tunyasuvunakool, K.; Wu, Z.; Zemgulyte, A.; Arvaniti, E.; Beattie, C.; Bertolli, O.; Bridgland, A.; Cherepanov, A.; Congreve, M.; Cowen-Rivers, A. I.; Cowie, A.; Figurnov, M.; Fuchs, F. B.; Gladman, H.; Jain, R.; Khan, Y. A.; Low, C. M. R.; Perlin, K.; Potapenko, A.; Savy, P.; Singh, S.; Stecula, A.; Thillaisundaram, A.; Tong, C.; Yakneen, S.; Zhong, E. D.; Zieliński, M.; Zidek, A.; Bapst, V.; Kohli, P.; Jaderberg, M.; Hassabis, D.; Jumper, J. M. Accurate structure prediction of biomolecular interactions with AlphaFold 3. *Nature* **2024**, *630* (8016), 493–500.
- (44) Leman, J. K.; Weitzner, B. D.; Lewis, S. M.; Adolf-Bryfogle, J.; Alam, N.; Alford, R. F.; Aprahamian, M.; Baker, D.; Barlow, K. A.; Barth, P.; Basanta, B.; Bender, B. J.; Blacklock, K.; Bonet, J.; Boyken, S. E.; Bradley, P.; Bystroff, C.; Conway, P.; Cooper, S.; Correia, B. E.; Coventry, B.; Das, R.; De Jong, R. M.; DiMaio, F.; Dsilva, L.; Dunbrack, R.; Ford, A. S.; Frenz, B.; Fu, D. Y.; Geniesse, C.; Goldschmidt, L.; Gowthaman, R.; Gray, J. J.; Gront, D.; Guffy, S.; Horowitz, S.; Huang, P. S.; Huber, T.; Jacobs, T. M.; Jeliazkov, J. R.; Johnson, D. K.; Kappel, K.; Karanicolas, J.; Khakzad, H.; Khar, K. R.; Khare, S. D.; Khatib, F.; Khrumishin, A.; King, I. C.; Kleffner, R.; Koepnick, B.; Kortemme, T.; Kuenze, G.; Kuhlman, B.; Kuroda, D.; Labonte, J. W.; Lai, J. K.; Lapidoth, G.; Leaver-Fay, A.; Lindert, S.; Linsky, T.; London, N.; Lubin, J. H.; Lyskov, S.; Maguire, J.; Malmstrom, L.; Marcos, E.; Marcu, O.; Marze, N. A.; Meiler, J.; Moretti, R.; Mulligan, V. K.; Nerli, S.; Norn, C.; O'Conchuir, S.; Ollikainen, N.; Ovchinnikov, S.; Pacella, M. S.; Pan, X.; Park, H.; Pavlovic, R. E.; Pethe, M.; Pierce, B. G.; Pilla, K. B.; Raveh, B.; Renfrew, P. D.; Burman, S. S. R.; Rubenstein, A.; Sauer, M. F.; Scheck, A.; Schief, W.; Schueler-Furman, O.; Sedan, Y.; Sevy, A. M.; Sgourakis, N. G.; Shi, L.; Siegel, J. B.; Silva, D. A.; Smith, S.; Song, Y.; Stein, A.; Szegedy, M.; Teets, F. D.; Thyme, S. B.; Wang, R. Y.; Watkins, A.; Zimmerman, L.; Bonneau, R. Macromolecular modeling and design in Rosetta: recent methods and frameworks. *Nat. Methods* **2020**, *17* (7), 665–680.
- (45) Namdar, A. H.; Zoghi, N.; Miller, A.; Saiani, A.; Shearer, T. Effects of fiber spatial distribution and relative orientation on the percolation and mechanics of stochastic fiber networks: A model of peptide hydrogels. *Phys. Rev. E* **2025**, *111* (6), 064407.